Applications and Health

Amygdalin functionalized carbon quantum dots for probing #-glucosidase activity for cancer diagnosis and therapeutics

Gopi Kalaiyarasan, Murugan Veerapandian, Gnanasekaran JebaMercy, Krishnaswamy Balamurugan, and James Joseph

ACS Biomater. Sci. Eng., **Just Accepted Manuscript** • DOI: 10.1021/acsbiomaterials.9b00394 • Publication Date (Web): 17 May 2019

Amygdalin Functionalized Carbon Quantum Dots for Probing β-Glucosidase Activity for Cancer Diagnosis and Therapeutics

Gopi Kalaiyarasan[§,¶], Murugan Veerapandian[§,¶], Gnanasekaran JebaMercy[†],

Krishnaswamy Balamurugan[†] and James Joseph[§,¶,*]

[§]Electrodics and Electrocatalysis division, CSIR-Central Electrochemical Research Institute (CECRI), Karaikudi- 630 003, India

[¶]Academy of Scientific & Innovative Research (AcSIR), CSIR-CECRI campus, Karaikudi-630 003, India

[†]Department of Biotechnology, Alagappa University, Science Campus, Karaikudi- 630 003, Tamil Nadu, India

***Address correspondence and reprint requests to:**

Dr. James Joseph,
Senior Principal Scientist,
Electrodics and Electrocatalysis division,
CSIR-Central Electrochemical Research Institute,
Karaikudi – 630003,
TamilNadu, India.
Contact numbers: +91 4565 241 330, +91 8903411735

or

Dr. James Joseph,
Professor,
Academy of Scientific & Innovative Research,
CSIR-Central Electrochemical Research Institute Campus,
Karaikudi – 630003,
TamilNadu, India.

Email: jameskavalam@yahoo.com; jamescecri@cecri.res.in

Abstract

Fluorescence active nanosystem capable of targeting specific receptors of cancer cells with or without bio-recognition element is advantageous for biosensor studies. Herein, a naturally occurring anti-cancer drug, amygdalin (synthetic form: Laetrile, a misnomer: vitamin B17) has been modified on the surface of carbon quantum dots, prepared by the hydrothermal method, to probe β-glucosidase activity. Despite its cyanide toxicity, amygdalin is recently revived to be an anti-cancer molecule, and the risk factor can be optimized by understanding its binding efficiency with β-glucosidase in the cancer cells. In this study, an *in vitro* bio-recognition pattern of amygdalin-functionalized carbon quantum dots (Amy@CQDs) toward β-glucosidase is typically evaluated by aggregation induced fluorescence emission mechanism. The optical functionality and structural integrity of CQDs before and after functionalization with amygdalin are comprehensively studied from spectroscopic and microscopic techniques. Our results demonstrate that Amy@CQDs is stable hydrophilic graphitic carbon nanostructure exhibiting selective fluorescence quenching upon interaction with β-glucosidase, enabling the lowest detection limit of 134 nM. Hydrolysis products of amygdalin mediated by β-glucosidase were further confirmed from HPLC and colorimetric method, indicating the selective binding of the prepared Amy@CQDs, which may find a useful application in cancer diagnosis and therapeutics.

Keywords: Amygdalin; β-glucosidase; Drug delivery; Carbon Quantum Dots; Aggregation-Induced Emission; Cancer diagnosis and therapeutics

1. Introduction

Amygdalin (Laetrile-synthetic form) is a cyanogenic glycoside found in kernels such as apricot, bitter almonds, apple, peach, clover, lima beans, sorghum, and plum[1]. It is widely used as a natural chemotherapy drug to cure cancer[2]. Further, it has other clinical importance

like immune function, anti-tussive, and anti-asthmatic property[2], kinase inhibitor[3]. However, early literature has revealed that amygdalin has toxicity issues while treating cancer patients[4]. Mainly, those patients had cyanide toxicity that was approaching the lethal range in blood. Due to this problem, the Food and Drug Administration (FDA) did not approve the amygdalin as a drug for cancer. Moreover, amygdalin has been classified as Poisonous Plant Kernels (FDA #: F08093).

However, in recent years, many studies demonstrated its anti-cancer activity including prostate cancer[5], bladder cancer[6], cervical cancer[7], breast cancer[8], colon cancer[9], rejuvenation of weakened kidney fibroblast and interstitial fibrosis[10]. The enzyme β-glucosidase governs the fundamental therapeutic function of amygdalin. Amygdalin splits into glucose molecules, benzaldehyde and cyanide ions through enzymatic hydrolysis by β-glucosidase[2,4,11]. The malignant neoplastic cells contain a large amount of β-glucosidase than normal cells[11]. Likewise, the concentration of rhodanese enzyme is very high in healthy cells than neoplastic cells. This enzyme converts the toxic hydrogen cyanide to non-toxic thiocyanic acid. Then thiocyanic acid is converted into vitamin B12 after several metabolic pathways. Due to those enzymes, the bio-converted cyanide species are selectively killing the cancer cells, and at the same time, the excess cyanide molecules are de-toxified by rhodanese enzyme[11]. From the above works of literature, it is clear that accurate determination of β-glucosidase has significant implications for clinical therapeutics particularly in the cancer treatment. Herein, the present study aimed to determine the *in vitro* concentration of β-glucosidase with high sensitivity as well as qualitative detection of enzymatic hydrolysis products (glucose, benzaldehyde, cyanide) of amygdalin. Beside cancer therapeutics, estimation of β-glucosidase also benefits alcoholic industries, because it has a vital role as flavor enhancement in beverages[12].

Similarly, β-glucosidase has another essential role in the isolation of bacteria[13] and detection of o-hydroxycinnamic acid in *Melilotus alba* leaves[14]. Few reports are available for

detection of β-glucosidase using polyacrylamide gel electrophoresis[15], spectrophotometric assay[16], fluorescence[14], colorimetry[17] techniques. Among them, the fluorescence-based approach has been invented to quantify biomolecules owing to its high sensitivity, ease of usage, simple system integration, and cost-efficient[18–20]. Many fluorescent probes such as organic/inorganic molecules/complex, dyes, noble metal clusters, quantum dots are used in analytical chemistry for the detection of the variety of analytes. Among them, quantum dots have high quantum yield, simple synthetic procedure, and high sensitivity towards analyte[21–24]. Many carbon-based quantum dots such as carbon quantum dots, graphene quantum dots, carbon nanodots have additional advantages like non-toxic, biocompatibility, resistance to photobleaching/blinking and inexpensive[25].

We have chosen carbon quantum dots with plenty of carboxylic acids on their surface which is accessible for functionalization with amygdalin *via* dehydration or esterification reaction. Trimesic acid was used as the precursor to prepare the CQDs with carboxylic acid groups on its surfaces. Experimental conditions like reaction time, temperature and precursor concentrations were optimized to obtain high quantum-yield CQDs. The CQDs have been functionalized with amygdalin in acidic condition. The CQDs and amygdalin functionalized carbon quantum dots (Amy@CQDs) were comprehensively characterized by various spectroscopic and electron microscopic techniques in order to understand the optical and structural properties. The determination of β-glucosidase was carried out by fluorescence technique using Amy@CQDs as the probe. The enzymatic activity of β-glucosidase toward hydrolysis of amygdalin on the surface of CQDs was evaluated by HPLC to validate the by-product benzaldehyde, while the formation of glucose moieties was ensured from Accu-Chek meter and conventional colorimetric assay.

2. Experimental

2.1. Materials

Trimesic acid (TMA), β-glucosidase, 0.2 μm PTFE syringe filter and cellulose dialysis tubing (2 kDa) were purchased from Sigma-Aldrich. Hydrochloric acid (HCl), Sodium hydroxide (NaOH), Sodium acetate, and Glacial Acetic acid were purchased from MERCK. All other chemicals were of analytical grade and used as received without further purification. All solutions were prepared with Milli-Q water (18.2 MΩ.cm). Cytotoxicity and *in vivo* measurement of *β*-glucosidase were performed using Hep3B liver cancer cell line.

2.2. Synthesis of CQDs

Series of CQDs have been synthesized using a series concentration of TMA at various reaction time and temperature (See Table S1). As-synthesized CQD's were purified with 0.2 μm PTFE syringe filter followed by 2 kDa cellulose dialysis tubing. Optical properties of these CQDs were analyzed with UV-vis and PL spectroscopy. Based on higher quantum yield (calculation described in SI 1.1), the synthesis procedure for the preparation of CQDs was optimized as follows. The 0.5 g of TMA dissolved in 30 mL of Milli-Q water and transferred to a 50 mL autoclave container. The autoclave was kept in the furnace at 190 °C for 12 h. The resultant solution was purified and kept for further studies.

2.3. Functionalization of amygdalin on CQDs

Functionalization of amygdalin on the surface of CQDs-modified with carboxylic acid groups were achieved through thermally controlled magnetic stirring at 70 °C for 1 h. For this, series of amygdalin (typically make the ratio of CQDs: amygdalin as 1:0.25, 1:1, 1:2, 1:3) was dissolved in each 5 mL of CQDs, and the pH was adjusted to 1.0 using HCl. This mixture was stirred for 1 h at 70 °C to carry out an esterification reaction. The resultant colloidal solution was dispersed in acetate buffer (pH = 4.5). As-resulted Amy@CQDs was analyzed by UV-vis

absorbance and PL spectroscopy. The highly fluorescent Amy@CQDs was taken for further spectroscopic, microscopic studies and analytical applications.

2.4. Determination of β-glucosidase and detection of glucose, benzaldehyde, and cyanide

6.75 mg of β-glucosidase dissolved in 5 mL of acetate buffer (pH=4.5) to make a stock solution (concentration of β-glucosidase is 10 μM). The appropriate volume of β-glucosidase added in 50 μL of Amy@CQDs in Costar 96 well microplate black flat bottom. The net volume of well maintained at 300 μL using acetate buffer (pH = 4.5). The final concentration of β-glucosidase range was maintained from 300 nM to 34 μM. This mixture was allowed to lysis for 30 min before record spectra. The PL spectra were recorded at 370 nm of excitation wavelength in the BioTek Synergy H1 instrument.

20 μL of Amy@CQDs before and after addition of 10 μM of β-glucosidase were taken for HPLC measurement using Phenomenex Phenogel 10u columns and HPLC grade methanol as eluent. Pure benzaldehyde diluted by methanol was used as a standard sample for confirmation. The same procedure followed for the detection of glucose using the Accu-Chek glucose meter and glucose colorimetric assay. The 10 μM of $FeSO_4$ added to the mixture of Amy@CQDs and β-glucosidase. We found the formation of Ferrocyanide by UV-vis spectrum. Then, we have added the 10 μM of $FeSO_4$ at the basic condition in the above mixture to confirm the formation of Prussian blue. UV-vis spectra of standard Ferrocyanide and Prussian blue analyzed.

2.5. β-glucosidase activity

Total β-glucosidase activity in the Hep3B liver cancer cells was measured using the β-Glucosidase Assay Kit (Sigma). The test samples' treated cell lysates were prepared by sonication in ice-cold PBS. After brief centrifugation, the supernatants were collected and stored. The assay was performed according to the manufacturer's protocol. The reactions were

carried out in the presence of NPG substrate and incubated at 37 °C for 20 minutes. The final absorbance was read at 405 nm[26].

2.6 MTT Assay

Percentage of cell viability was measured using Vybrant® MTT Cell Proliferation Assay kit (V-13154, Thermo Fisher Scientific). Briefly, 10^4 cells (Hep3B) were seeded in a 96-well plate for 24 h and undergone for treatment with test samples. At first, a dose-dependent study was performed with various concentrations (10, 100 and 1000 µg/mL). After treatment the cell viability was determined at different time intervals such as 1 h, 6 h, and 12 h. 10 µL of MTT reagent (12 mM) was added in all the wells at the mentioned period and the cells were incubated for 4 h at 37 °C. Then the resulted formazan crystals were dissolved by the addition of 50 µL of DMSO (Sigma) and taken for absorbance measurement at 540 nm using a multi-plate reader (SpectraMax M3)[27]. Each data point denotes the average of three independent experiments.

3. Results and Discussion

3.1. Synthesis of CQDs

The UV-vis absorbance and PL spectra of CQDs synthesized by various experimental conditions were shown in Fig. S1a & b. The fluorescence quantum yield was calculated and tabulated in Table S1. From the results, it can be suggested that the fluorescence intensity and QY were increased with increasing concentration of TMA. However, the high concentration of TMA (1.0 g in 30 mL) does not allow the complete carbonization under hydrothermal method possibly due to the limitation of solubility of TMA. Similarly, low reaction temperature (160 °C) and time (6 h) are not sufficient to create CQDs effectively. On the other hand, higher reaction time (24 h) is also ineffective to produce fluorescent CQDs. Therefore, we found the highly fluorescent, π-conjugated, graphitized CQDs from 0.5 g of TMA under the hydrothermal

treatment at 190 ºC for 12 h. This CQD used for spectroscopic, microscopic characterizations and functionalization for the biomedical applications.

3.2. UV-vis and PL studies of CQDs and Amy@CQDs

The UV-Vis absorbance of CQDs is shown in Fig. 1A (a). It has absorption at wavelength starting from 300 nm to 350 nm attributed to π–π* and n–π* of the central core of graphitized CQDs due to C=O functional groups on its surfaces[25]. In contrast, TMA did not show that absorbance (Fig. S2), and the absorbance of molecular chromophores such as aromatic C–C bond and C=O bond occurred at 210 nm and 284 nm. These peaks can be assigned to π–π* and n–π* electronic transitions[28]. Generally, an increasing amount of conjugated π electrons leads to a redshift in absorbance wavelength. Further, the UV-vis absorbance spectra of Amy@CQDs comprising 1:1 ratio are illustrated in Fig. 1A(b). For better understanding, the absorbance spectra of Amy@CQDs at different ratios (1:0.25, 1:1, 1:2 and 1:3) were also performed, which are represented in supporting information as Fig. S3 (a). It is interesting to note that the intensity of inherent absorbance peak around 280 nm observed from the aqueous dispersion of Amy@CQDs was found to increase with increasing the concentration of amygdalin. Perhaps this observation could be related to the dissociation of the intermolecular hydrogen bond, existing in the CQDs. To ensure this, an additional study on the intrinsic absorbance spectrum of aqueous amygdalin was performed (Fig. S4), which has no noticeable absorption around 280 nm. Further, unlike pristine CQDs, the absorbance spectra of Amy@CQDs around 320 nm was noticeably different. Similar dissociation of intermolecular hydrogen bond mediated absorbance and blue shift in the absorbance wavelength were discussed in the literature[29]. Therefore, the peak at 280 nm can be assigned to the characteristic absorbance of Amy@CQDs, indicating the formation of the ester bond *via* dehydration.

The PL spectra of CQDs taken by various excitation wavelengths are depicted in Fig. 1B. The fluorescence emission at 430 nm was unchanged with an excitation wavelength range from 200 nm to 400 nm. The maximum emission intensity was observed at 430 nm with an excitation wavelength of 340 nm as plotted in Fig. 1A (c). The λ_{ex}-independent fluorescence emission at 430 nm indicates that the fluorescence emission originated from the central core of the graphitized CQDs due to π–π* electronic transition. The n–π* of the C=O of carboxylic groups did not involve in the fluorescence emission. If the fluorescence originates by molecular chromophore like C=O which is combined with aromatic C–C connections, it is expected to be λ_{ex}-dependent fluorescence emission[28]. The fluorescence lifetime of CQDs is 5.5 ns, calculated from the fluorescence decay curve as shown in Fig. 1C. The decay curve was obtained at excitation/emission wavelengths of 340/430 nm and fitted by a single exponential function. Therefore, the CQDs is a single fluorescent component which means the CQDs do not have surface states/defects. Many reports in the literature describe that oxidized carbon dots show the λ_{ex}-dependent emission due to surface states/defects[21,30,31]. We have synthesized un-doped and oxidized CQDs with unusual fluorescence effect of λ_{ex}-independent emission which is again clearly proved that the origin of fluorescence is due to the central core of CQDs or quantum/size effect without surface defect/states like semiconductor quantum dots[21]. The PL spectra of Amy@CQDs at different ratios (1:0.25, 1:1, 1:2 and 1:3) at different excitation wavelengths ranging from 350 nm to 530 nm are shown in Fig. S5a-d. From the experimental investigation, it is observed that the 370 nm of excitation wavelength gives the maximum fluorescence emission intensity at 520 nm. Further, among the tested concentrations, 1:1 ratio of Amy@CQDs was exhibiting the superior emission intensity (Fig. S3b). Thus, further investigations were performed using the 1:1 ratio of Amy@CQDs. As shown in Fig.1d, the fluorescence emission wavelength of Amy@CQDs was shifted from 430 nm to 520 nm after functionalization. This observation confirms the interaction of amygdalin on CQDs perhaps

via the dehydration reaction. Moreover, the shift in emission wavelength is ascribed to the aggregation-induced emission (AIE). Similar observations were reported in tetraphenylethene based fluorescent compound *via* esterification/dehydration reaction with glucose[32]. The aggregation of CQDs through dehydration with amygdalin were further confirmed by HRTEM studies described in section 3.4.

3.3. FTIR and XPS studies of CQDs and Amy@CQDs

The FTIR spectrum of CQDs (Fig. 2a) shows the characteristic peaks at 1637 cm^{-1}, 1703 cm^{-1}, 3467 cm^{-1} these are assigned to stretching frequency of C=C, C=O, O–H groups. The FTIR spectrum of TMA show the same characteristic peaks at different wave numbers, i.e., 1627 cm^{-1} and 1699 cm^{-1} for stretching vibrational frequencies of C=C and C=O bonds Fig. S6. Compared to TMA, we have found the increased stretching frequency of C=C and C=O for CQDs due to increased bond strength or graphitization that confirming the formation of CQDs. Moreover, the transmittance ratio of C=C/C=O is significantly higher in CQDs than in TMA. Because the C=C present in central core and C=O present only in the extrinsic core of CQDs. It is strongly recommended that the size of the product (CQDs) is higher than precursor (TMA) and the amount of C=C bonds is higher than C=O bonds. The proposed dehydration reaction between CQDs and amygdalin was confirmed by FTIR spectroscopy. The FTIR spectrum of Amy@CQDs (Fig. 2b) showing the characteristic peak at 1724 cm^{-1} that can be attributed to C=O stretching, similar to CQDs exhibiting the vibration ~1703 cm^{-1} (Fig. 2a). The observed shift in the frequency (~20 cm^{-1}) confirmed the formation of the ester linkage. Distinct from pristine amygdalin (Fig. S7), Amy@CQDs has a significant increase in the transmittance of C-O stretching and bending vibration around 1031 cm^{-1} and 1244 cm^{-1}, respectively (Fig. 2b). Observed FTIR vibrational information denotes the successful functionalization of amygdalin on the surface of CQDs *via an* esterification reaction.

To complement FTIR results, an XPS analysis was performed to ensure the presence of functional groups on CQDs and functionalization with amygdalin through the formation of the ester bond. Fig. S8 shows the full survey spectrum of CQDs which show two characteristic peaks at 285 eV and 532 eV due to C_{1s} and O_{1s} respectively. The Fig. 2c shows the C_{1s} peak that can be deconvoluted into four peaks, by Gaussian fit, at 284.6 eV, 285.8 eV, 287.3 eV, and 289.6 eV which are assigned to aromatic C–C/C=C, C–O, C=O and COOH groups respectively[25]. At the same time, the C_{1s} spectrum of Amy@CQDs can be deconvoluted into four peaks centered at 284.3 eV, 285.8 eV, 287.5 eV, and 288.7 eV, which can be assigned to aromatic C–C/C=C, C–O, C=O, and O=C–OR (ester) bond, respectively as shown in Fig. 2d. The carboxylic acid peak appeared at 289.6 eV in CQDs that is shifted to lower energy (288.7 eV) in Amy@CQDs due to the existence of the ester bond after functionalization. Similarly, the O_{1s} peak of CQDs can be deconvoluted into two peaks at 531.0 eV, and 532.4 eV are assigned to C=O and C–O–H/C–O–C groups (Fig. 2e). Additionally, the existence of C–O–C bond has been proved by the O_{1s} spectrum of Amy@CQDs (Fig. 2f). The intensity at 532.1 eV due to C–O–C is increased in Amy@CQDs than CQDs. These functional groups offer superior water solubility, and stability.

3.4. HRTEM analyses of CQDs and Amy@CQDs

The high-resolution transmission electron microscope (HRTEM) images and SAED pattern of CQDs are depicted in Fig. 3a-c. The CQDs are self-assembled like a polymer matrix probably due to intermolecular hydrogen bond, prevailing between carboxylic acid groups (Fig. 3a). Generally, the carboxylic acid groups can make an intermolecular hydrogen bond. Additionally, the CQDs are self-assembled through dehydration/anhydride formation between carboxylic acid groups of adjacent CQDs while drying the sample after drop casting. The average size of CQDs calculated as 5.0 nm from the normal distribution curve of the histogram of Fig. 3a and the histogram plotted as an inset of Fig. 3a. At higher magnification, we have

found the fringes with different planes (Fig. 3b). The d-spacing of 1.26 Å, 1.64 Å, and 2.10 Å can be assigned to (110), (004) and (100) planes of the hexagonal crystalized, graphitized carbon (JCPDS: 00-001-0640). Moreover, the SAED pattern (Fig. 3c) of CQDs confirms the existence of graphitized carbon through the formation nanocrystalline ring with the d-spacing of 2.10 Å, which is assigned to (100) plane of the graphitized carbon. Therefore, from the data obtained from the imaging and diffraction analyses, it is clear that the formed material is monodispersed crystalline and highly ordered graphitized carbon quantum dots. The HRTEM image of Amy@CQDs is shown in Fig. 3d, which depicts the formation of larger nanoclusters, due to the aggregation of surface-bound amygdalin (Fig. S9a-b). From Fig. S9(c), the surface topography of the nanoclusters is observed to have quantum dots upon higher magnification. From the selected area of HRTEM image, the average particle size of CQDs and Amy@CQDs were analyzed using image J software which was found to be <5 nm, suggesting the existence of nanoscale distribution even after functionalization (Fig. S9d).

From the above spectroscopic (UV-vis, PL, FTIR, and XPS) and electron microscopic (HRTEM and SAED) investigations, it is clear that the amygdalin is effectively functionalized on CQDs *via* dehydration/esterification reaction, with a capability of generating an AIE, prospective fluorescence-based probe for sensor applications.

3.5. Effect of pH on the optical functionality of CQDs

The UV-vis absorbance spectra of CQDs at pH range from 2.0 to 12.0 were shown in Fig. 4a. The absorbance around 320 nm due to π–π electronic transition was decreased with increase in the pH from 2.0 to 7.0 due to deprotonation of C=O groups. The protonation will affect the π–π electronic transition than n–π transition in CQDs due to the negative mesomeric effect of pronated carboxylic acid groups. Thus, the intensity of absorption at 320 nm increased with decreasing pH. After pH 7.0, the absorbance was shifted to 330 nm of wavelength, which

absorbance is continuously increased with increasing pH due to the functional groups that are deprotonated and enhancing the electron density of π–π system in the central core of CQDs due to positive mesomeric effect. Therefore, the absorbance shifted and rose at 330 nm. It is significantly affecting the fluorescence emission as shown in Fig. 4b. The carboxylate groups at higher pH have enhanced the fluorescence intensity due to higher net surface charge that provides the CQDs with hydrophilic properties, aqueous stability, and dispersibility, subsequently enhancing the PL intensity[33]. At the same time, we have observed the enhancement in fluorescence intensity with decreasing pH from 7.0 to 2.0, which is in good agreement with the literature[29]. Pan et al. have reported the same results for fluorescent nanoparticles, but the exact mechanism was not described[34]. Konkena et al. reported the red shift in fluorescence but without incremental changes in the absorbance spectra of graphene oxide dispersions[29]. Choudhury et al. demonstrated the fluorescence changes concerning pH in lemon derived dots due to the formation of chemically different species[35]. From the present experimental results, we have demonstrated that the protonation/deprotonation is significantly inducing the conjugated π system/localization due to the mesomeric effect[25]. Such a mesomeric effect is ineffective at neutral pH, which is reflected by the lower fluorescence intensity. The concentration of H^+ and OH^-may involve in the electronic transition variations of π-π* and n–π* in CQDs by refilling or depleting their valence band[36]. The observation associated with the surface modification with a carboxylic acid which is acting as pH-sensing groups *via* protonation and deprotonation. The presence of pH-sensitive groups of CQDs is further confirmed by zeta potential measurement. The zeta potential of as prepared CQDs (pH is 3.0) is –1.3 mV. The zeta potential of CQDs at pH 2.0 is 1.8 mV, and it is decreased to –35.4 mV (pH 12.0) with increasing pH that is adjusted using HCl and NaOH (Fig. 4c). Based on the observed results, we believe that the formed CQDs are carboxylic acid terminated, graphitized, crystalline, pH sensitive, hydrophilic, stable and monodispersed nanosystem with a fluorescent

functionality. The fluorescence originates from the central core of CQDs due to quantum confinement effect, it is affected by auxochromes (carboxylic acid), and these are responsible for the pH sensor.

3.6. Detection of hydrolyzed products of amygdalin

In order to understand the catalytic activity of β-glucosidase on amygdalin, we have analyzed the enzymatic hydrolysis products of amygdalin such as glucose, benzaldehyde, and hydrogen cyanide (Scheme. 1). The release of glucose from this mixture was determined by Accu-Chek glucose meter and a standard colorimetric method (Glucose test kit (GOD-POD) was used based on Trinder's method). In the presence of β-glucosidase, the experimental concentration of glucose derived from Amy@CQDs using Accu-Chek meter was found to be 8.5 mM, while in the absence ofβ-glucosidase it was 0 mM. In the case of colorimetric method, the glucose concentration derived from Amy@CQDs without β-glucosidase and with β-glucosidase was measured to be 1.3 mM and 11.2 mM, respectively. The 1.3 mM of glucose concentration found in the Amy@CQDs before the addition/reaction of β-glucosidase is perhaps due to the limitation of Trinder's method.

HPLC studies confirmed the presence of benzaldehyde, the enzymatic hydrolysis product of amygdalin. Initially, 20 μL of Amy@CQDs was injected for the HPLC measurement. We have found a peak at a retention time of 3.6th minute (Fig. 5a). Then 20 μL of a mixture of Amy@CQDs and β-glucosidase (incubated about 30 minutes before the analysis) was injected. We have found three peaks at a retention time of 3.4th, 3.1st, and 2.6th minutes (Fig. 5a). To identify the peaks, we ran benzaldehyde as a reference. The benzaldehyde peak appeared at the 3.4th minute of retention time (Fig. 5b). The existence of benzaldehyde is evidenced by the enzymatic hydrolysis reaction between amygdalin and β-glucosidase. The other peaks can be attributed to hydrolysis fragments of Amy@CQDs by β-glucosidase.

The existence of other enzymatic hydrolysis products of amygdalin, *i.e.,* cyanide was confirmed by UV-vis spectroscopy through the formation of iron-cyanide complex and Prussian blue[37]. The UV-vis spectra of Amy@CQDs with β-glucosidase depicted in Fig. 5c shows a new broad peak around 340 nm in the presence of $FeSO_4$. At the same time, neither pristine $FeSO_4$ aqueous solution (Fig. 5d) nor the Amy@CQDs with β-glucosidase (Fig. 5c) does not exhibit the absorbance at 340 nm. This distinct observation confirms that only the existence of free CN^- ions mediated the formation of ferrocyanide, $[Fe(CN)_6]^{4-}$ complex and its respective absorbance at 340 nm. Moreover, the formation of ferrocyanide complex was also evidenced by the UV-vis spectrum of pure potassium ferrocyanide used as a reference (Fig. 5d). In order to further make sure the existence of $[Fe(CN)_6]^{4-}$ complex, a reaction with $FeSO_4$ at pH 8.0 was performed which will assist the formation of Prussian blue. The color of *in-situ* generated ferrocyanide complex is turned to blue, which enable a new absorbance around 750 nm (Fig. 5c). This peak is distinctly attributed to Prussian blue, in agreement with standard reference shown in Fig. 5d. From the visible absorbance-based evidence, it is confirmed that enzymatic hydrolysis products (*viz.,* glucose, benzaldehyde, and cyanide) of amygdalin is generated upon selective chemical interaction with β-glucosidase. Therefore, the as-prepared Amy@CQDs could be a selective fluorescent probe for the determination of β-glucosidase and has promising feasibility as a diagnostic probe as well as a drug carrier for cancer/anti-neoplastic therapy.

3.7. Determination of β-glucosidase

It is known that the enzymatic hydrolysis reaction of amygdalin using β-glucosidase will give the glucose, benzaldehyde and hydrogen cyanide as per Scheme. 1 at acidic condition ($pH < 4.5$)[11]. Importantly the glycoside bond (ester bond in Amy@CQDs) will be broken down by β-glucosidase. Therefore AIE is weakened concerning the concentration of β-glucosidase owing to dissociation of CQDs and amygdalin that leads to quenching in the AIE. Based on

this mechanism, we have added 300 nM to 34 μM of β-glucosidase in Amy@CQDs. The PL intensity of Amy@CQDs at 520 nm of emission wavelength was gradually decreased with β-glucosidase when excited at 370 nm (Fig. 6a). From this spectrum, we have calculated the binding constant (K) using the Lineweaver-Burk equation (Eq. 1) as described below,

$$\frac{1}{F_0 - F} = \frac{1}{F_0} + \frac{1}{KF_0[Q]} \quad \textbf{Eq. 1}$$

Where F and $F_0$are the fluorescence intensity of the Amy@CQDs in presence and absence of β-glucosidase, and [Q] is the concentration of β-glucosidase, the K value is 2.78 × 10^5 M^{-1} as calculated from Fig. 6b using Eq. 1. Our method is superior to other research which shows the binding constant of β-glucosidase in glucose-6-phosphate activated *Bacillus polymyxa* as 4.0 × 10^4 M^{-1} [38]. Further, the limit of detection and Stern-Volmer quenching constant also calculated from the Stern-Volmer plot (Fig. 6c) as 134 nM and 2.23 × 10^5, respectively. Very few reports are available for the detection of β-glucosidase[14–17]. Compared to those reports, our method is simple, reliable, inexpensive, and sensitive.

3.8. Determination of β-glucosidase in Hep3B cell line using Amy@CQDs

Determination of β-glucosidase in cancer cell line by the proposed method is validated, and its accuracy was compared with the results of the β-glucosidase Activity Assay Kit. Standard addition method was followed for the detection of β-glucosidase. The fluorescence intensities were measured at excitation/emission wavelengths of 370/520 nm for a mixture of Hep3B cell line and Amy@CQDs in the presence of different concentrations of β-glucosidase (2, 3 and 4 μM), in addition to control. These values were plotted in Fig. 7a from which the concentration of β-glucosidase in Hep3B was found to be 2.9 μM. Based on the available literature data on healthy cells,[39] Hep3B cancer cells are studied to have three-order higher concentration of β-glucosidase.

3.9. Determination of β-glucosidase in Hep3B cell line using commercial assay kit

Existence of β-glucosidase in Hep3B cancer cells was quantified using β-Glucosidase Activity Assay Kit. Fig. 7b illustrates the concentration of β-glucosidase in Hep3B cells before and after 12 h treatment with CQDs, amygdalin, and Amy@CQDs. The β-glucosidase present in the control sample was found to be 8.75±0.28 units/L. After addition of 100 μg/mL of CQDs to cancer cell line, the concentration of β-glucosidase is reduced to 7.75±0.69 units/L, perhaps due to inherent adsorption of proteins (β-glucosidase) on carbon materials. In the case of amygdalin, residual β-glucosidase concentration was found to be 8.64±0.65 units/L, which is around 1.04 units/L difference in comparison with control cells. Unlike other test samples, the Amy@CQDs treated Hep3B cell lines exhibited the lowest β-glucosidase concentration, *i.e.,* 1.28±1.8 units/L. From the observed result, it is clear that the hydrolysis reaction of β-glucosidase is superior with Amy@CQDs. As discussed earlier the hydrolyzed products of amygdalin such as cyanide and benzaldehyde moieties may involve in the anti-cancer activity.

In order to get further information on the drug-cell interaction, a confocal Raman microscopic analysis was performed, and the results are provided in supporting information, from Fig. S10. It can be observed that the amide-I functional groups of protein moieties in amygdalin treated Hep3B cells are weakly resolved at 1115 cm^{-1}.[40] In the case of CQDs and Amy@CQDs treated Hep3B cells the amide-I bands were well resolved and appeared to be broadened with a notable shift to 1161 and 1221 cm^{-1}, respectively. This change indicates the existence of multiple amide-I functional groups. It is speculated that the interaction of CQDs and Amy@CQDs perhaps altered the cellular components which resulted into formation of disintegrated protein fragments. From the observed result, it is evident that the prepared CQDs and Amy@CQDs effectively interacted with the Hep3B cells than the pristine amygdalin. C=O vibrations from the Hep3B cells treated with amygdalin and CQDs were identified at 1682 cm^{-}

[1], while the Amy@CQDs interacted sample exhibit the relevant signal at 1692 cm^{-1} with a significant broadness. The peak observed at 1899 cm^{-1} from the Amy@CQDs treated Hep3B cell line is assigned to C=O groups, which is distinct and not appeared in the other two samples. This may result from one of the hydrolyzed products of amygdalin, i.e., benzaldehyde. All other bands observed at lower wavenumbers remain the same without significant changes.

3.10. Anti-cancer Activity of Amy@CQDs

Anticancer mechanism of action of amygdalin *via* β-glucosidase is still unclear because of controversial debate. In this study, Hep3B liver cancer cell lines were tested with prepared CQDs and Amy@CQDs. At first, the cell viability was measured using MTT cell proliferation assay kit. For this purpose, different concentrations of the prepared samples were tested (10, 100 and 1000 μg/mL) and incubated for 12 h (Fig. 7c). From the histogram it is observed that CQDs treated Hep3B cells are exhibited decreased cell viability with an increase of CQDs concentration, denoting 72.8% viability with 1000 μg/mL. Interestingly the amygdalin interacted cells are showing better cell proliferation (82 to 98%) with higher concentrations. It may be since the weak adsorption behavior of amygdalin mediated a poor interaction with Hep3B cells. In the case of Amy@CQDs, the cell viability of Hep3B cells is significantly decreased indicating the better anti-cancer activity. It may be noticed that with high concentration (1000 μg/mL) of Amy@CQDs the viability is slightly improved. In order to further understand this particular phenomenon, a time-dependent cell cytotoxicity assay was performed. Fig. 7d illustrates the cell viability percentage at three-time intervals such as 1, 6, and 12 h. From the histogram, it is clear that pristine CQDs and amygdalin does not have significant toxicity at the present studied concentration (100 μg/mL). Distinctly Amy@CQDs exhibit superior anticancer activity (14% at 1 h, 7.8% at 6 h and 6.2% at 12 h) compared to other samples. From the experimental results, it is evident that Amy@CQDs exhibit

synergistic combination supporting the controlled release of hydrolyzed products of amygdalin.

4. Conclusions

Highly fluorescent carboxylic acid terminated CQDs were prepared from the trimesic acid by hydrothermal method. The λ_{ex}-independent fluorescence emission originates from the central core of the graphitized crystalline CQDs by the quantum confinement effect. The fluorescence emission of CQDs is pH sensitive due to the presence of carboxylic acid on the surface of CQDs, facilitating the functionalization of an anti-cancer drug (amygdalin) *via* dehydration. Efficient changes in optical absorbance/emission and structural integrity ensures the surface modification of CQDs. The AIE of Amy@CQDs shows an inherent potentiality toward β-glucosidase detection. Binding constant and Stern-Volmer quenching constant of the Amy@CQDs upon interaction with β-glucosidase is studied *via* fluorescence quenching, with a detection limit of 134 nM (S/N ratio = 3). The enzymatic hydrolysis products of amygdalin were sequentially confirmed by colorimetric, HPLC, Accu-Chek, and glucose assay kit. The Amy@CQDs system displayed advantages for its ease in preparation and operation, stable graphitic carbon structure exhibiting pH and λ_{ex}-independent fluorescence emission property and hence selective for tracing β-glucosidase in a concentration-dependent manner. Studies on the *in vivo* probing of β-glucosidase in Hep3B cell lines also supported the observation that the developed Amy@CQDs exhibit selective recognition. Moreover, the anti-cancer functionality of Amy@CQDs is found to be superior compared to pristine CQDs and amygdalin. Obtained results suggest that the prepared hybrid Amy@CQDs may find utility in both diagnosis of β-glucosidase in cancer cells and time-dependent anti-cancer therapeutics.

Acknowledgments

Gopi Kalaiyarasan thanks the Joint CSIR-UGC, India for Senior Research Fellowship. M. Veerapandian acknowledges the support of the Department of Science and Technology, India for the DST-Inspire Faculty award (DST/INSPIRE/04/2015/002081). Authors acknowledge the laboratory assistance rendered by Mr. Venkata Krishna, Department of Biotechnology, Alagappa University. Authors also acknowledge the support of Dr. B. Subramanian and their team of CSIR-CECRI for rendering their facility to check the cancer cell line functions.

Appendix A. Supporting information

The spectroscopic and microscopic techniques, sample preparation for characterization, quantum yield calculation and additional figures with discussion were presented in supporting information.

References

(1) Bolarinwa, I. F.; Orfila, C.; Morgan, M. R. A. Amygdalin Content of Seeds, Kernels and Food Products Commercially-Available in the UK. *Food Chem.* **2014**, *152*, 133–139. doi:10.1016/J.FOODCHEM.2013.11.002

(2) Song, Z.; Xu, X.; Song, Z. Advanced Research on Anti-Tumor Effects of Amygdalin. *J. Cancer Res. Ther.* **2014**, *10* (5), 3. doi:10.4103/0973-1482.139743.

(3) Kim, M.; Rangasamy, S.; Shim, Y.; Song, J. Cell Lysis-Free Quantum Dot Multicolor Cellular Imaging-Based Mechanism Study for TNF-α-Induced Insulin Resistance. *J. Nanobiotechnology* **2015**, *13* (1), 4. doi:10.1186/s12951-015-0064-x.

(4) Moertel, C. G.; Fleming, T. R.; Rubin, J.; Kvols, L. K.; Sarna, G.; Koch, R.; Currie, V. E.; Young, C. W.; Jones, S. E.; Davignon, J. P. A Clinical Trial of Amygdalin (Laetrile) in the Treatment of Human Cancer. *N. Engl. J. Med.* **1982**, *306* (4), 201–206.

doi:10.1056/NEJM198201283060403.

(5) Chang, H.-K.; Shin, M.-S.; Yang, H.-Y.; Lee, J.-W.; Kim, Y.-S.; Lee, M.-H.; Kim, J.; Kim, K.-H.; Kim, C.-J. Amygdalin Induces Apoptosis through Regulation of Bax and Bcl-2 Expressions in Human DU145 and LNCaP Prostate Cancer Cells. *Biol. Pharm. Bull.* **2006**, *29* (8), 1597–1602. doi:10.1248/bpb.29.1597. doi:10.1371/journal.pone.0105590.

(6) Makarević, J.; Rutz, J.; Juengel, E.; Kaulfuss, S.; Reiter, M.; Tsaur, I.; Bartsch, G.; Haferkamp, A.; Blaheta, R. A. Amygdalin Blocks Bladder Cancer Cell Growth in Vitro by Diminishing Cyclin A and Cdk2. *PLoS One* **2014**, *9* (8).

(7) Chen, Y.; Ma, J.; Wang, F.; Hu, J.; Cui, A.; Wei, C.; Yang, Q.; Li, F. Amygdalin Induces Apoptosis in Human Cervical Cancer Cell Line HeLa Cells. *Immunopharmacol. Immunotoxicol.* **2013**, *35* (1), 43–51. doi:10.3109/08923973.2012.738688.

(8) Zhou, X.; Huang, Z.; Yang, H.; Jiang, Y.; Wei, W.; Li, Q.; Mo, Q.; Liu, J. β-Glucosidase Inhibition Sensitizes Breast Cancer to Chemotherapy. *Biomed. Pharmacother.* **2017**, *91*, 504–509. doi:10.1016/j.biopha.2017.04.113.

(9) Elbossaty, W. F. Mechanism Action of Amygdalin as Natural Chemotherapy in Colon Cancer. *Res. Rev. J. Pharmacol. Toxicol. Stud.* **2018**, *6* (1), 47–51.

(10) Guo, J.; Wu, W.; Sheng, M.; Yang, S.; Tan, J. Amygdalin Inhibits Renal Fibrosis in Chronic Kidney Disease. *Mol. Med. Rep.* **2013**, *7* (5), 1453–1457. doi:10.3892/mmr.2013.1391.

(11) Shalayel, M. H. F. Beyond Laetrile (Vitamin B-17) Controversy-Antitumor Illusion or Revolution. *Br. Biomed. Bull.* **2017**, *5* (1), 296.

(12) Lomolino, G.; Zocca, F.; Spettoli, P.; Lante, A. Detection of β-Glucosidase and Esterase Activities in Wild Yeast in a Distillery Environment. *J. Inst. Brew.* **2006**, *112* (2), 97–100. doi:10.1002/j.2050-0416.2006.tb00237.x.

(13) Veena. Isolation and Characterization of β-Glucosidase Producing Bacteria from Different Sources. *AFRICAN J. Biotechnol.* **2011**, *10* (66), 14907–14912. doi:10.5897/AJB09.314.

(14) Haskins, F. a; Gorz, H. J. Rapid Detection of σ-Hydroxycinnamic Acid and Beta-Glucosidase in Melilotus Alba1. *Crop Sci.* **1970**, *10* (5), 479. doi:10.2135/cropsci1970.0011183X001000050006x.

(15) Kwon, K.; Lee, J.; Kang, H. G.; Chil, Y. Detection of β -Glucosidase Activity in Polyacrylamide Gels with Esculin as Substrate Detection of 3-Glucosidase Activity in Polyacrylamide Gels with Esculin as Substrate. *Appl. Environ. Microbiol.* **1994**, *60* (12), 4584–4586.

(16) Stradwick, L.; Inglis, D.; Kelly, J.; Pickering, G. Development and Application of Assay for Determining β-Glucosidase Activity in Human Saliva. *Flavour* **2017**, *6* (1), 1. doi:10.1186/s13411-017-0054-z.

(17) Edberg, S. C.; Trepeta, R. W.; Kontnick, C. M.; Torres, A. R. Measurement of Active Constitutive ??-D-Glucosidase (Esculinase) in the Presence of Sodium Desoxycholate. *J. Clin. Microbiol.* **1985**, *21* (3), 363–365.

(18) Kalaiyarasan, G.; K, A.; Joseph, J. Melamine Dependent Fluorescence of Glutathione Protected Gold Nanoclusters and Ratiometric Quantification of Melamine in Commercial Cow Milk and Infant Formula. *Appl. Surf. Sci.* **2017**, *420*, 963–969. doi:10.1016/j.apsusc.2017.05.193.

(19) Kalaiyarasan, G.; Narendra Kumar, A. V.; Sivakumar, C.; Joseph, J. Photoluminescence of Oligomers of Aniline-2-Sulfonic Acid Formed in the Presence of AuCl4− and Sodium Citrate: Application in the Optical Detection of Hemoglobin. *Sensors Actuators B Chem.* **2015**, *209*, 883–888. doi:10.1016/j.snb.2014.12.041.

(20) Veerapandian, M.; Zhu, X. X.; Giasson, S. Chitosan-Modified Silver@ruthenium Hybrid Nanoparticles: Evaluation of Physico-Chemical Properties and Bio-Affinity with Sialic Acid. *J. Mater. Chem. B* **2015**, *3* (4), 665–672. doi:10.1039/c4tb01475h.

(21) Lim, S. Y.; Shen, W.; Gao, Z. Carbon Quantum Dots and Their Applications. *Chem. Soc. Rev.* **2014**, *44* (1), 362–381. doi:10.1039/c4cs00269e.

(22) Kalaiyarasan, G.; Joseph, J. Cholesterol Derived Carbon Quantum Dots as Fluorescence Probe for the Specific Detection of Hemoglobin in Diluted Human Blood Samples. *Mater. Sci. Eng. C* **2019**, *94*, 580–586. doi:10.1016/j.msec.2018.10.007.

(23) Kalaiyarasan, G.; Hemlata, C.; Joseph, J. Fluorescence Turn-On, Specific Detection of Cystine in Human Blood Plasma and Urine Samples by Nitrogen-Doped Carbon Quantum Dots. *ACS Omega* **2019**, *4* (1), 1007–1014. doi:10.1021/acsomega.8b03187.

(24) Kalaiyarasan, G.; Joseph, J. Efficient Dual-Mode Colorimetric/Fluorometric Sensor for the Detection of Copper Ions and Vitamin C Based on PH-Sensitive Amino-Terminated Nitrogen-Doped Carbon Quantum Dots: Effect of Reactive Oxygen Species and Antioxidants. *Anal. Bioanal. Chem.* **2019**, *411* (12), 2619–2633. doi:10.1007/s00216-019-01710-8.

(25) Kalaiyarasan, G.; Joseph, J. Determination of Vitamin B12 via PH-Dependent Quenching of the Fluorescence of Nitrogen Doped Carbon Quantum Dots. *Microchim. Acta* **2017**, *184* (10), 3883–3891. doi:10.1007/s00604-017-2421-y.

(26) Henriques, A.; Huebecker, M.; Blasco, H.; Keime, C.; Andres, C. R.; Corcia, P.; Priestman, D. A.; Platt, F. M.; Spedding, M.; Loeffler, J.-P. Inhibition of Beta-Glucocerebrosidase Activity Preserves Motor Unit Integrity in a Mouse Model of Amyotrophic Lateral Sclerosis. *Sci. Rep.* **2017**, *7* (1), 5235. doi:10.1038/s41598-017-05313-0.

(27) Bou Assaf, R.; Fayyad-Kazan, M.; Al-Nemer, F.; Makki, R.; Fayyad-Kazan, H.; Badran, B.; Berberi, A. Evaluation of the Osteogenic Potential of Different Scaffolds Embedded with Human Stem Cells Originated from Schneiderian Membrane: An In Vitro Study. *Biomed Res. Int.* **2019**, *2019*, 2868673. doi:10.1155/2019/2868673.

(28) Liu, Y.; Liu, C. Y.; Zhang, Z. Y. Synthesis and Surface Photochemistry of Graphitized Carbon Quantum Dots. *J. Colloid Interface Sci.* **2011**, *356* (2), 416–421. doi:10.1016/j.jcis.2011.01.065.

(29) Konkena, B.; Vasudevan, S. Spectral Migration of Fluorescence in Graphene Oxide Aqueous Dispersions: Evidence for Excited-State Proton Transfer. *J. Phys. Chem. Lett.* **2014**, *5* (1), 1–7. doi:10.1021/jz4024755.

(30) Li, L.; Li, L.; Wang, C.; Liu, K.; Zhu, R.; Qiang, H.; Lin, Y. Synthesis of Nitrogen-Doped and Amino Acid-Functionalized Graphene Quantum Dots from Glycine, and Their Application to the Fluorometric Determination of Ferric Ion. *Microchim. Acta* **2014**, *182* (3–4), 763–770. doi:10.1007/s00604-014-1383-6.

(31) Sun, Y. P.; Zhou, B.; Lin, Y.; Wang, W.; Fernando, K. a S.; Pathak, P.; Meziani, M. J.; Harruff, B. a.; Wang, X.; Wang, H.; et al. Quantum-Sized Carbon Dots for Bright and Colorful Photoluminescence. *J. Am. Chem. Soc.* **2006**, *128* (24), 7756–7757. doi:10.1021/ja062677d.

(32) Liu, Y.; Deng, C.; Tang, L.; Qin, A.; Hu, R.; Sun, J. Z.; Tang, B. Z. Specific Detection

of D-Glucose by a Tetraphenylethene-Based Fluorescent Sensor. *J. Am. Chem. Soc.* **2011**, *133* (4), 660–663. doi:10.1021/ja107086y.

(33) Yang, G.; Wan, X.; Su, Y.; Zeng, X.; Tang, J. Acidophilic S-Doped Carbon Quantum Dots Derived from Cellulose Fibers and Their Fluorescence Sensing Performance for Metal Ions in an Extremely Strong Acid Environment. *J. Mater. Chem. A* **2016**, *4* (33), 12841–12849. doi:10.1039/C6TA05943K.

(34) Pan, D.; Zhang, J.; Li, Z.; Wu, C.; Yan, X.; Wu, M. Observation of PH-, Solvent-, Spin-, and Excitation-Dependent Blue Photoluminescence from Carbon Nanoparticles. *Chem. Commun. (Camb).* **2010**, *46* (21), 3681–3683. doi:10.1039/c000114g.

(35) Dutta Choudhury, S.; Chethodil, J. M.; Gharat, P. M.; Praseetha, P. K.; Pal, H. PH-Elicited Luminescence Functionalities of Carbon Dots: Mechanistic Insights. *J. Phys. Chem. Lett.* **2017**, *8* (7), 1389–1395. doi:10.1021/acs.jpclett.7b00153.

(36) Chen, J.-L.; Yan, X.-P. Ionic Strength and PH Reversible Response of Visible and Near-Infrared Fluorescence of Graphene Oxide Nanosheets for Monitoring the Extracellular PH. *Chem. Commun. (Camb).* **2011**, *47* (11), 3135–3137. doi:10.1039/c0cc03999c.

(37) Adams, M. D. The Removal of Cyanide from Aqueous Solution by the Use of Ferrous Sulphate. *J. South. African Inst. Min. Metall.* **1992**, *92* (1), 17–25.

(38) Weiss, P. H. E.; Álvares, A. C. M.; Gomes, A. A.; Miletti, L. C.; Skoronski, E.; da Silva, G. F.; de Freitas, S. M.; Magalhães, M. L. B. Beta Glucosidase from Bacillus Polymyxa Is Activated by Glucose-6-Phosphate. *Arch. Biochem. Biophys.* **2015**, *580*, 50–56. doi:10.1016/j.abb.2015.06.012.

(39) Pastores, G. M.; Hughes, D. A. *Gaucher Disease*; Adam, M. P., Ardinger, H. H.,

Pagon, R. A., Wallace, S. E., Bean, L. J. H., Stephens, K., Amemiya, A., Eds.; Seattle (WA), 1993.

(40) De Luca, A. C.; Dholakia, K.; Mazilu, M. Modulated Raman Spectroscopy for Enhanced Cancer Diagnosis at the Cellular Level. *Sensors (Switzerland)* **2015**, *15* (6), 13680–13704. doi:10.3390/s150613680.

For Table of Contents Use Only

Amygdalin Functionalized Carbon Quantum Dots for Probing β-Glucosidase Activity for Cancer Diagnosis and Therapeutics

Gopi Kalaiyarasan[§,¶], Murugan Veerapandian[§,¶], Gnanasekaran JebaMercy[†], Krishnaswamy Balamurugan[†] and James Joseph[§,¶,*]

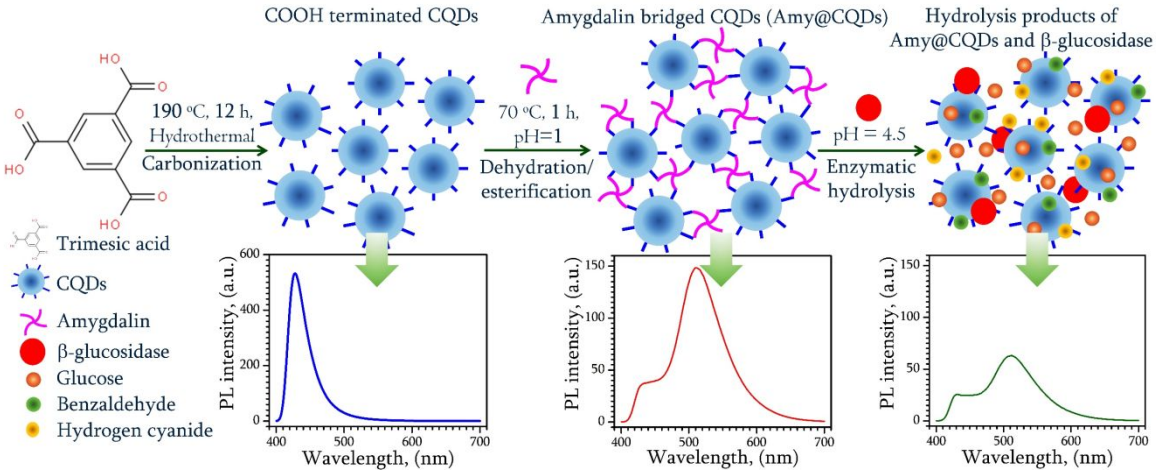

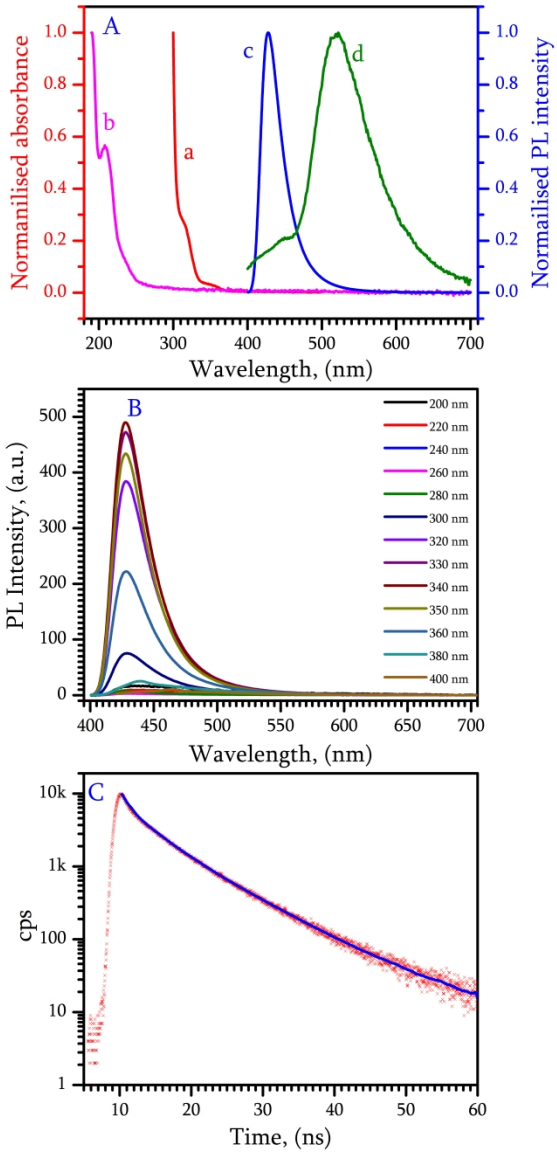

Fig. 1A (a and b) UV-vis absorbance spectra and (c and d) PL spectra of CQDs and Amy@CQDs respectively. The excitation wavelengths are 340 nm and 370 nm for CQDs and Amy@CQDs respectively. (B) PL spectra of CQDs at various excitation wavelength starting from 200 nm to 400 nm, (C) Fluorescence lifetime decay profile of CQDs at excitation/emission wavelengths of 340/430 nm.

938x1944mm (96 x 96 DPI)

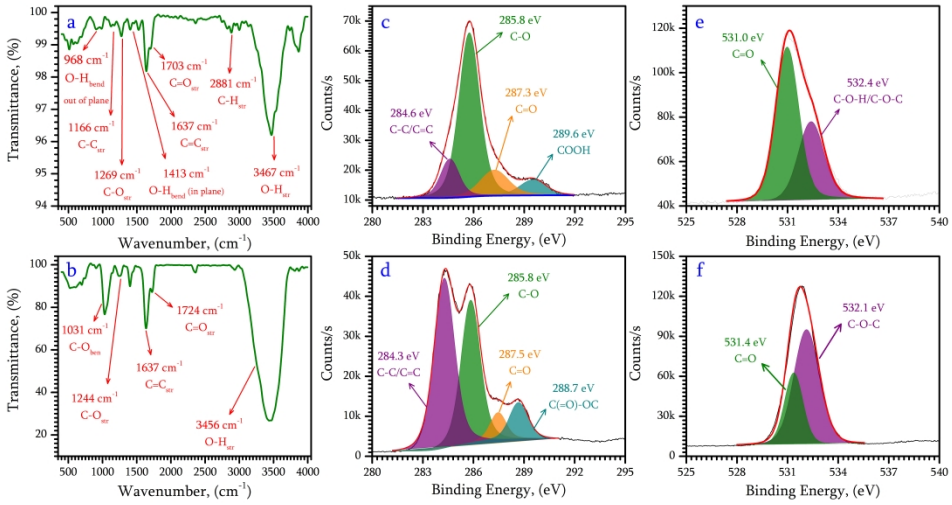

Fig. 2 (a and b) FTIR, (c and d) C1s, (e and f) O1s deconvoluted XPS spectra of CQDs and Amy@CQDs respectively.

2092x1107mm (96 x 96 DPI)

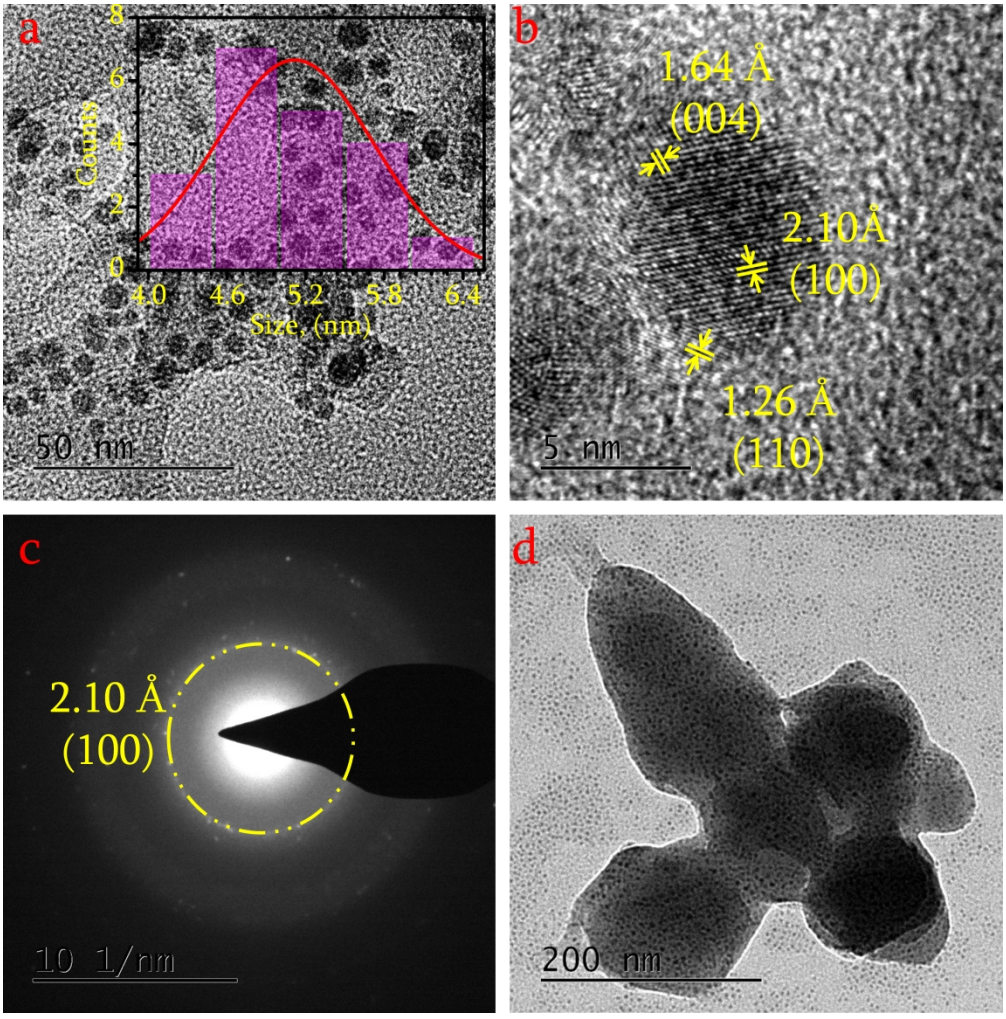

Fig. 3 The HRTEM image of CQDs (a) at low magnification and (b) at high magnification and (c) the SAED pattern of CQDs and (d) the HRTEM image of Amy@CQDs. The inset of (a) shows the size distribution histogram for the corresponding picture.

1358x1368mm (96 x 96 DPI)

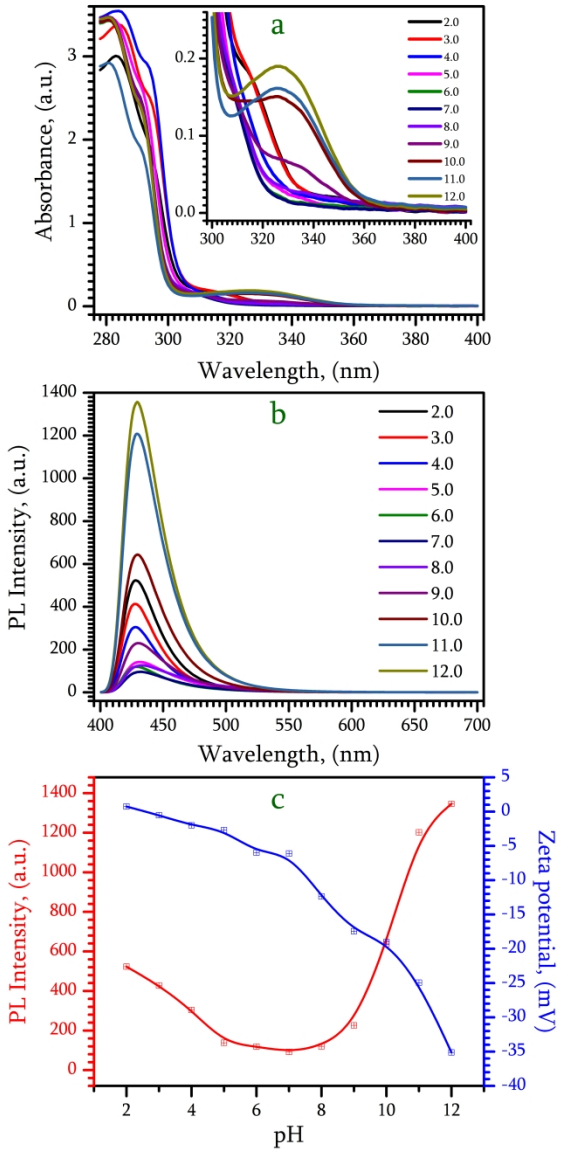

Fig. 4 (a) The UV-vis and (b) PL spectra of CQDs at various pH range from 2.0 to 12.0 and (c) the plot of PL emission intensity at 430 nm and Zeta potential of CQDs at various pH. The excitation wavelength is 340 nm.

1005x2105mm (96 x 96 DPI)

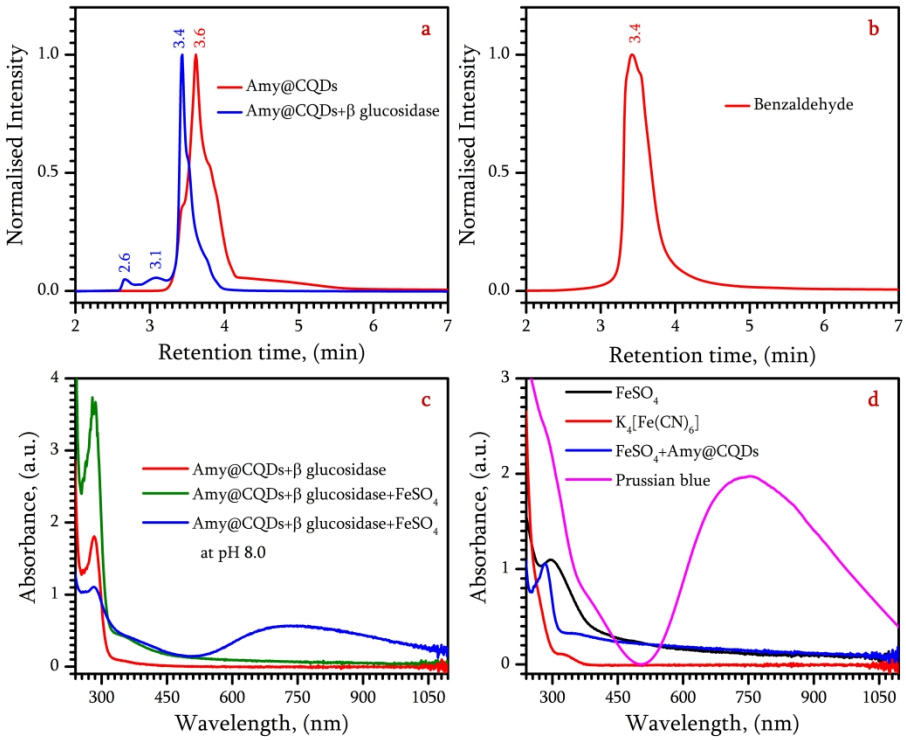

Fig. 5 HPLC chromatogram of (a) Amy@CQDs with/without β–glucosidase, (b) benzaldehyde as reference, UV-vis spectra of (c) Amy@CQDs with β–glucosidase in presence of FeSO4 at acidic pH (to confirm the formation of [Fe(CN)6]4– complex) and at basic pH (to confirm the formation of Prussian blue) and (d) Free FeSO4, Prussian blue, Ferrocyanide, Amy@CQDs with FeSO4 for reference.

1583x1237mm (96 x 96 DPI)

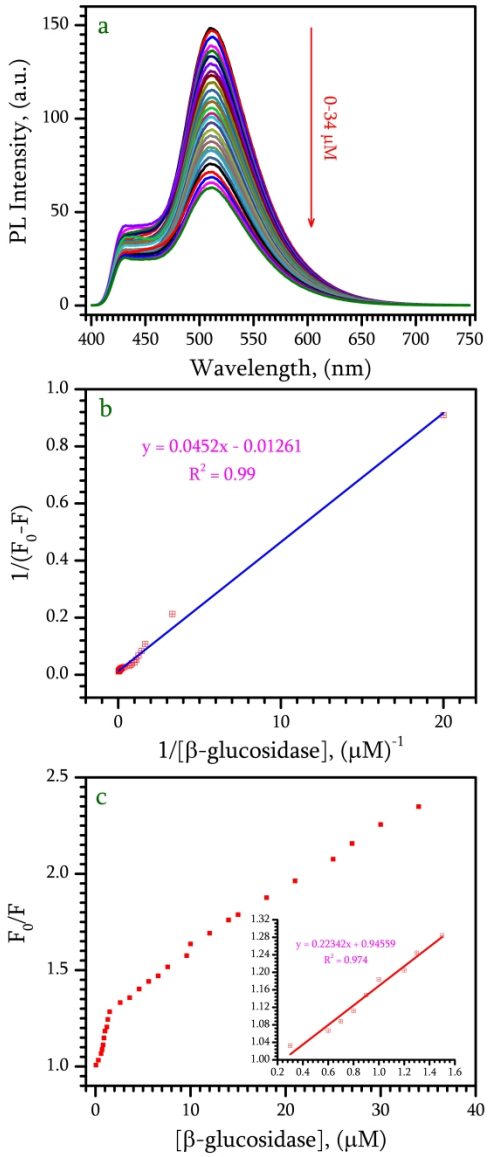

Fig. 6 (a) The PL spectra of Amy@CQDs in presence/absence of β–glucosidase concentration range from 300 nM to 34 μM at the excitation wavelength of 370 nm, (b) Lineweaver–Burk plot, (c) Stern Volmer plot obtained from the graph (a). The inset of (c) represents the linearity for β–glucosidase determination.

1086x2277mm (96 x 96 DPI)

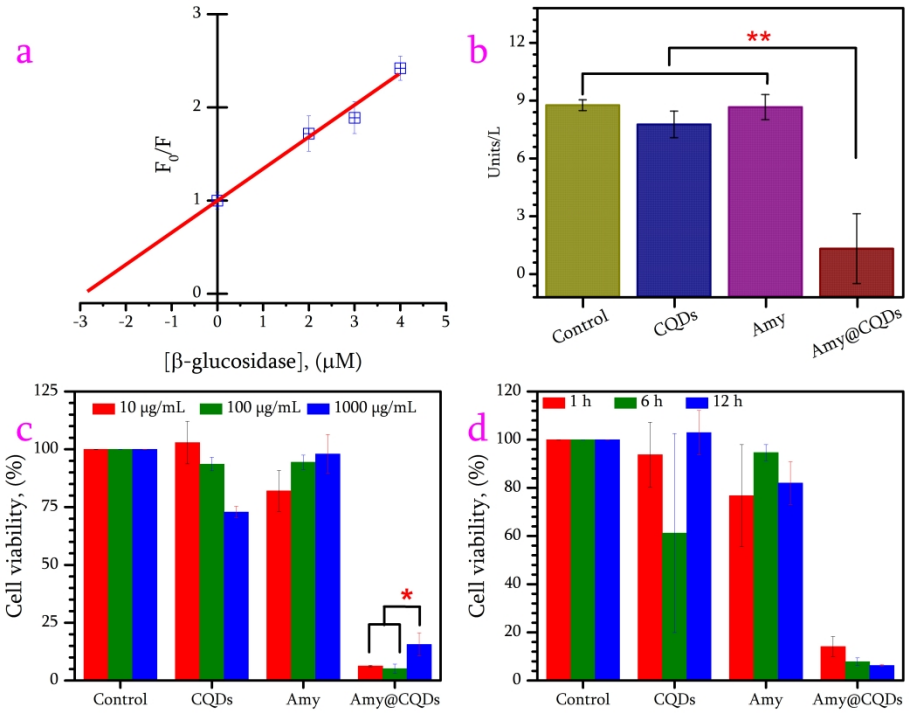

Fig. 7 (a) The standard addition curve for the detection of β–glucosidase in Hep3B cell line, (b) concentration of β–glucosidase in Hep3B cell line in presence of CQDs, amygdalin, Amy@CQDs, and cell viability of Hep3B cell line with (c) increasing concentration and (d) increasing time. All the statistical analysis was performed by one-way ANOVA and observed to be significant at the level of <0.005 (**) and < 0.05 (*).

1484x1133mm (96 x 96 DPI)

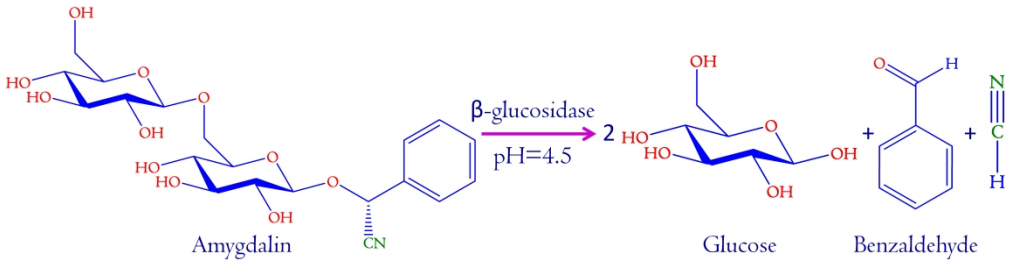

Scheme 1. Enzymatic hydrolysis reaction of Amygdalin by β-glucosidase

2287x617mm (96 x 96 DPI)

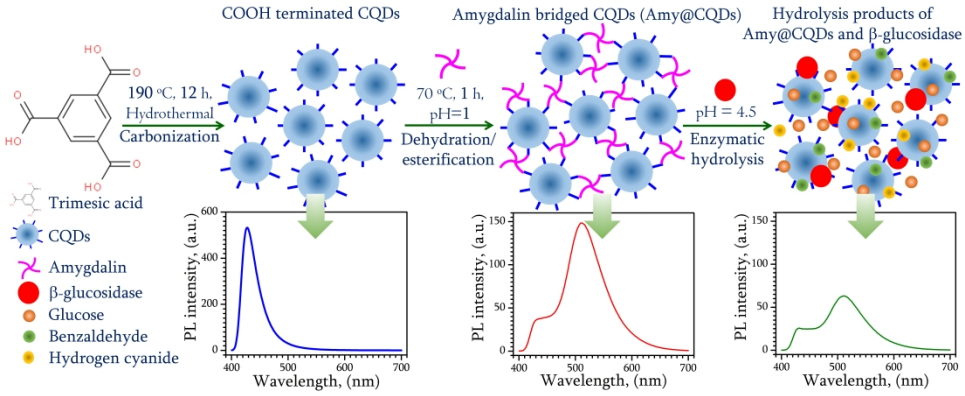

Table of Contents graphic

2419x951mm (96 x 96 DPI)